IET Electrical Systems in Transportation

Research Article

IET Journals
The Institution of Engineering and Technology

Distance-oriented hierarchical control and ecological driving strategy for HEVs

ISSN 2042-9738
Received on 1st July 2018
Revised 15th September 2018
Accepted on 16th October 2018
E-First on 9th January 2019
doi: 10.1049/iet-est.2018.5044
www.ietdl.org

Bowen Zhang[1], Hansang Lim[2], Shengyao Xu[1], Wencong Su[1] ✉

[1]Electrical and Computer Engineering Department, University of Michigan-Dearborn, Dearborn, USA
[2]Department of Electronics Convergence Engineering, Kwangwoon University, Seoul, Republic of Korea
✉ *E-mail: wencong@umich.edu*

Abstract: Hybrid electric vehicles (HEVs) provide a promising alternative to conventional engine-powered vehicles, with less emission and better fuel economy. This study proposes a hierarchical control for a power-split HEV over a driving cycle, featuring pre-trip optimisation and en-route speed adaption. Constraints including vehicle powertrain boundaries, road gradients, and speed limits, are taken into consideration. In the first stage, the HEV operating conditions, including the optimal vehicle SOC, speed profiles, and total driving time, are generated for the entire trip before departure. Based on the pre-trip results, the second stage adapts the vehicle speed for a short horizon when driving, while taking the safety spacing to the preceding vehicle into consideration, which acts as an indicator of actual traffic conditions and guarantees safe driving. Both optimisations are conducted under the distance domain for realising localisation in the optimal speed profile due to frequent changes in traffic conditions. An estimation of distribution algorithm is used to run the simulation so that the feasibility, robustness, and effectiveness of the proposed hierarchical control can be demonstrated.

1 Introduction

Due to increasing energy demand and environmental concerns, mean for achieving less emissions and higher fuel efficiency have become a popular research trend for the development of vehicles in the automobile industry. Hybrid electric vehicles (HEVs) and plug-in HEVs (PHEVs) have been considered as promising candidates to improve fuel economy while satisfying the tightened emission requirements [1]. Among three hybrid powertrain configurations, namely, series, parallel, and power-split, the power-split is considered as the combination of parallel and series designs [2]. By splitting torque properly between an internal combustion engine and an electrical motor in the powertrain, this configuration manages to satisfy the power demand efficiently. However, to reach a significant improvement on the fuel consumption and gas emission, a comprehensive energy control strategy is required for this power-split configuration.

Power-split HEV energy management algorithms can be classified into two categories: rule-based strategies and optimisation-based algorithms [3]. Rule-based control strategies are normally based on deterministic [4, 5] or fuzzy rules [6]. In [4], a hybridised rule-based with the global positioning system (GPS) approach for HEV in urban area is proposed. The daily driving fuel consumption and emissions are reduced. A real-time energy management strategy which combines rule-based control and equivalent consumption minimisation strategy is introduced in [5] for HEVs. Different driving cycles are implemented to verify its effectiveness. The advantages of rule-based strategies are their simplicity in execution and the ability in real-time performance. However, rules pre-defined by human expertise or heuristic methods usually result in inflexibility, and final results are not guaranteed to be optimal.

When applied to HEVs and PHEVs, optimisation-based strategies are generally categorised into: global optimisation and real-time optimisation [7]. In global optimisation, a cost function is usually defined using historical data such as vehicle speed, acceleration, and deceleration, battery state-of-charge (SOC) profile. In [8], the dynamic programming (DP) algorithm is implemented to obtain the global optimum of a power-split HEV. Prokhorov [9] used DP results as a benchmark for the HEV optimal control. However, DP is not a causal solution since it requires full knowledge of the entire trip. In [10–13], equivalent consumption minimisation strategy method is conducted for real-time application purpose. This algorithm uses an equivalent index between electricity and fuel consumption to minimise the cost function. Other methods such as model predictive control (MPC) [14, 15] and stochastic dynamic programming are also employed [16, 17].

Historical profiles including vehicle data and traffic data can be easily available in advance thanks to the development of GPS. Many papers have been studied to utilise these information into the HEV optimisation problem. In [18], authors optimise the minimal fuel consumption given a road gradient profile. A MPC-based HEV energy management strategy is proposed in [19] to reach a lower emission and global battery SOC variance. Sun *et al*. [20] collected real-time traffic data to regulate the vehicle SOC trajectory.

Therefore, HEV energy management with multi-stage control and optimisation has emerged to improve the performance and reduce computational time [21–24]. Simulation result from the previous level is able to provide inferences for the following one, so as to improve model accuracy and robustness. Huang [23] offered a multi-level control strategy for a parallel HEV by applying the improved particle swarm optimisation algorithm. Wang *et al*. [24] introduced an upper layer control to obtain the HEV optimal speed and battery energy profiles, a middle layer to determine the engine and gear on/off switches, and a lower layer to manage acceleration request between power sources.

Nevertheless, since vehicle fuel consumption is dependent on the characteristics of the powertrain, along with the operating conditions according to trip and traffic information and driving patterns [25, 26], only current or historical data are used in different driving cycles, which cannot always guarantee an efficient driving for vehicles with different powertrains. Moreover, most existing HEV power management strategies are based on the time domain where changes in traffic conditions and differences in HEV powertrain are not taken into account. In [27], a driver's pedal position map indicating vehicle acceleration/deceleration at every second is generated to identify an equilibrium operating condition at each time frame. In [28], the authors investigate the HEV fuel brake torque and battery SOC performance with 20 min driving under different driving cycles. However, those generated or

© The Institution of Engineering and Technology 2018

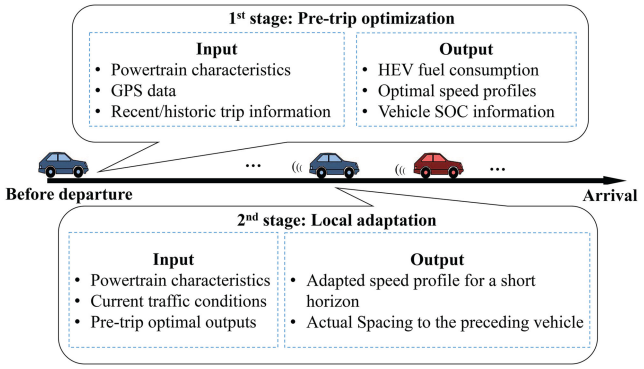

Fig. 1 *Two-stage optimisation under a distance domain*

optimised HEV variables such as vehicle speed and/or battery SOC profiles for an entire trip cannot maintain valid as long as the traffic condition change happens. For example, if any optimisation or adaptation of the vehicle speed is performed due to traffic condition or speed limit change, then all the speed values after the adjusted time period need to be updated as well, even if this period is very short compared to the entire driving time. Consequently, the remaining speed profile is required to be calculated again. Moreover, since traffic condition changes happen frequently, the speed profile is normally calculated back and forth, such that the entire computational cost of the hierarchical control turns out to be extremely large, which is not desirable for ecological driving [26].

In order to take the advantages of multi-level control and overcome the abovementioned limitations, this paper proposes a distance-based hierarchical control for a power-split HEV, including pre-trip optimisation and en-route speed adaption. Constraints due to vehicle powertrain limits, road gradients, and speed limits are considered. In the first stage, the HEV operating conditions, including the optimal vehicle SOC, speed profiles, and total driving time, are generated for the entire trip before departure. Based on the pre-trip results, the second stage adapts the vehicle speed for a short horizon when driving, while the safety spacing to the preceding vehicle is taken into consideration, which acts as an indicator of actual traffic conditions and guarantees safe driving. Both optimisations are conducted under the distance domain for realising localisation in the optimal speed profile due to frequent changes in traffic conditions. An estimation of distribution algorithm (EDA) is implemented to run the simulation, and a genetic algorithm (GA) is set to be the benchmark so that the feasibility, robustness, and effectiveness of the proposed hierarchical control can be demonstrated.

The major contributions of this paper are as follows:

- A hierarchical control strategy for a power-split HEV is formulated under distance domain in order to maintain the optimality under changeable traffic conditions. The characteristics of the HEV drivetrain, along with the traffic and trip information are considered.
- From the global perspective, the proposed approach generates not only the optimal vehicle speed and total driving time, but also the HEV battery SOC profiles for the entire trip, which ultimately guides the HEV user to drive in a more ecological fashion;
- From the local perspective, an en-route speed adaptation is applied based on the optimal results generated from the pre-trip stage. A safe driving is guaranteed by considering real-time traffic conditions and the distance to the preceding vehicle.

The remainder of this paper is organised as follows. Section 2 will describe the distance-based mathematical formulation. The authors will provide the vehicle model for the power-split HEV, objective functions, and system constraints for both stages. Section 3 will review the EDA methods, as well as describe how this algorithm is implemented for the proposed hierarchical control problem. The results and analysis of the simulation are presented in Section 4. Finally, the authors will summarise the paper in Section 5.

2 Problem formulation

2.1 Hierarchical optimisation under the distance domain

As in Fig. 1, the proposed hierarchical optimisation consists of two stages. In the first stage, an optimal vehicle speed and SOC profile for an entire route are generated. Historic traffic information, such as road gradients, speed limits, and so on, and the characteristics of the HEV drivetrain are considered. This stage is conducted prior to the vehicle's departure so that the optimised results can be used as reference profiles.

The second stage is performed after the HEV's departure. The spacing to the preceding vehicle is considered as an indicator of smooth or congested traffic conditions. Then, the vehicle speed is adapted by taking actual changes in real traffic conditions into consideration. Since traffic condition, especially in city areas, change frequently, the second stage speed control is conducted for a very short horizon. A shorter computational time can be obtained compared with that of the long-term first stage, so that the second stage has the potential to be implemented as a real-time control.

In the distance domain, when a speed adjustment happens, only the speeds of surrounding segments are changed, since they are directly affected by traffic conditions. For the remaining route, the original computed speed profile is still effective. For example, as long as the heavy traffic regions are not too wide, and there are few traffic signals on the driving route, the computational cost of every speed adjustment is small and the rest of the speed profile can be maintained. This improvement in computational cost explains the reason for conducting hierarchical control under the distance domain [26].

2.2 First stage: pre-trip SOC and speed optimisation

In this sub-section, the proposed distance-based power-split HEV model for pre-trip optimisation is introduced. The first-stage objective function and its constraints are also presented.

The proposed pre-trip optimisation is performed before the HEV's departure. Fig. 2 illustrates an example route for the proposed distance-based pre-trip optimisation. The entire route length is divided into several segments under the distance domain. The total driving time for the entire trip is estimated. An expected optimal speed profile, as well as the vehicle's SOC information for all locations, are generated by applying characteristics of the power-split HEV powertrain, driver-oriented data (e.g. final destination, recent trip information, driver's own preferences) and standard data (e.g. GPS data, weather conditions, road conditions, speed limits).

The objective function considered in the first stage optimisation is the minimisation of J. As shown in (1), there are two terms in the objective function. The first term mainly considers on the HEV fuel cost, where m_{f} stands for the vehicle fuel rate, and Δt_k represents the time difference, which is expressed in (4); the second term considers the vehicle speed deviation. The objective function intends to make the practical vehicle speed value as close as possible, to the target speed v_{ref}. Fig. 3 illustrates an example of the target speed profile under the distance domain. Including the starting point, the entire driving route in this stage is divided into $(N+1)$ locations, with an identical distance of Δs between each location. Consequently, the total distance of the driving cycle is $N\Delta s$. ω_1 and ω_2 are weighting factors for each term

$$\min J = \omega_1 \sum_{k=1}^{N} m_{\mathrm{f}}(k)\Delta t_k + \omega_2 \sum_{k=1}^{N} [v_{\mathrm{ref}}(k) - v(k)]^2 \tag{1}$$

$$m_{\mathrm{f}} = f(\omega_e, T_e) = [\alpha_1\omega_e(k) + \alpha_2]T_e(k) + \beta_1\omega_e(k) + \beta_2 \tag{2}$$

$$T_e(k) = f[\omega_e(k), P_{\mathrm{batt}}(k), F_{\mathrm{brake}}(k), v(k-1), v(k)] \tag{3}$$

$$\Delta t_k = t(k+1) - t(k) = \frac{2\Delta s}{v(k) + v(k+1)} \tag{4}$$

The engine speed ω_e, the vehicle battery power P_{batt}, the brake force F_{brake}, and the vehicle speed v are considered as the input

© The Institution of Engineering and Technology 2018

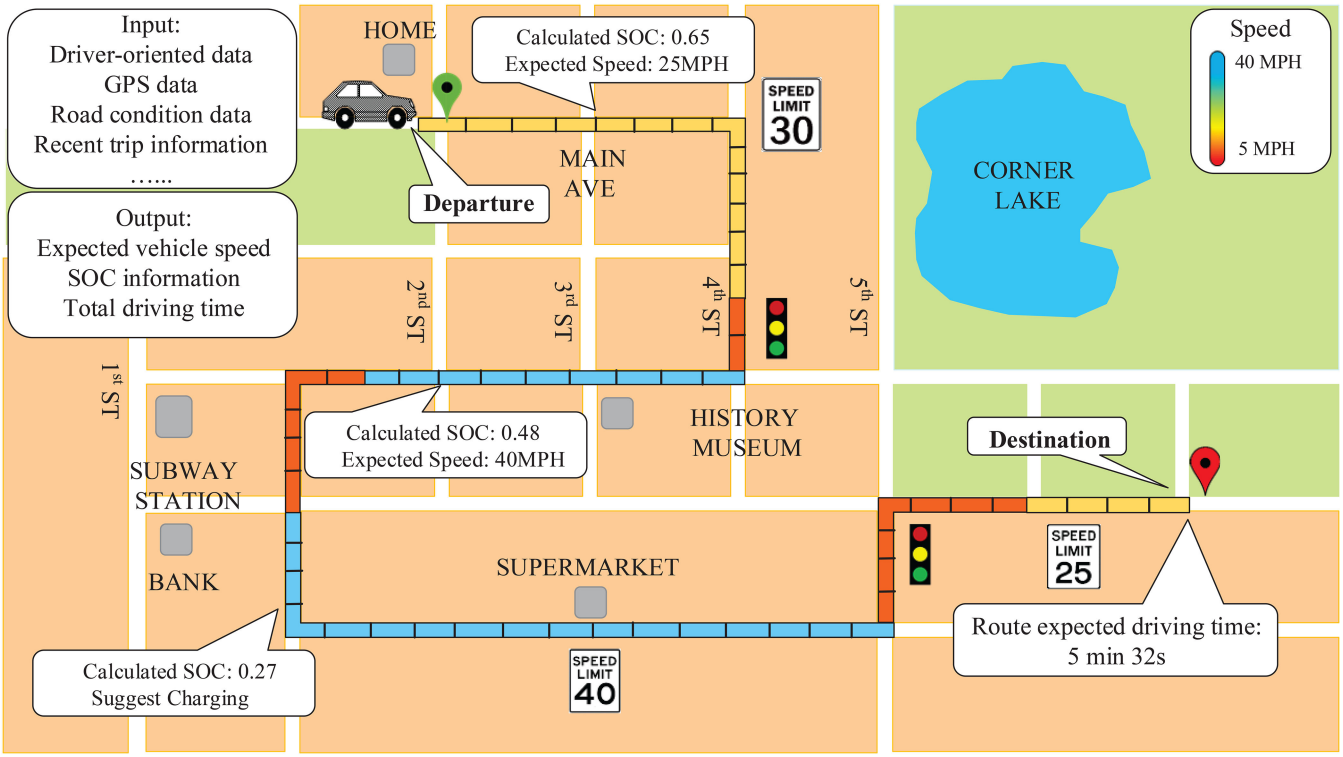

Fig. 2 *Example route for the distance-based pre-trip optimisation*

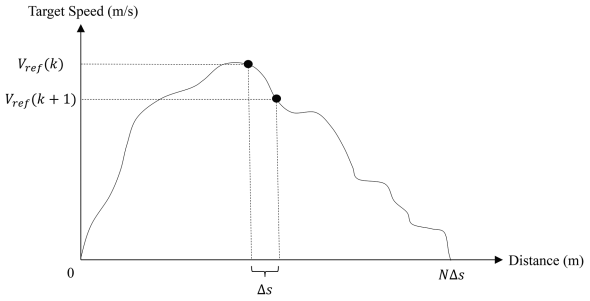

Fig. 3 *Target speed profile in the distance domain*

variables. Based on the Willans line approximation method [29], the vehicle fuel rate m_f can be expressed by the engine rotational speed ω_e and the engine torque T_e, as shown in (2), where α_1, α_2, β_1, and β_2 are constants. Furthermore, (3) shows that the engine torque T_e is a function of the first four abovementioned variables. The detailed expression of T_e is derived by the following procedure.

Both (5) and (6) describe the torque relationship inside the HEV powertrain model. T_e can be denoted by either the ring gear torque T_{ring}, or the generator torque T_{gen}. N_r and N_s are the number of teeth of the ring and sun gear, respectively. In order to simplify the formulation, the moment of inertia for the engine and motor are ignored, and λ represents the teeth ratio between the ring gear and the sun gear

$$T_e(k) = \frac{N_r + N_s}{N_r} T_{\text{ring}}(k) = (1+\lambda) T_{\text{ring}}(k) \tag{5}$$

$$T_e(k) = \frac{N_r + N_s}{N_s} T_{\text{gen}}(k) = \left(1 + \frac{1}{\lambda}\right) T_{\text{gen}}(k) \tag{6}$$

$$T_{\text{demand}}(k) = T_{\text{ring}}(k) + T_{\text{motor}}(k) = \frac{1}{1+\lambda} T_e(k) + T_{\text{motor}}(k) \tag{7}$$

Both the ring gear and the vehicle motor are connected to the final driveline, which means the final torque demand of the vehicle consists of the ring gear torque T_{ring} and the motor torque T_{motor}.

Table 1 Constant parameter values

Parameters	Values
m	1607 kg
R_{wheel}	0.30115 m
ρ	1.19854 kg/m^3
C_d	0.3
A_d	2.25084 m^2
g	9.81 m/s^2

Thus, (7) can be obtained. To denote T_e, the expressions for T_{demand} and T_{motor} should be obtained first.

In order to derive another equation for the final torque demand T_{demand}, vehicle dynamic equation (8) is applied, where $C_1 = 1/R_{\text{wheel}}$, $C_2 = (1/2)\rho C_d A_d$, and $C_3 = mgC_r\cos\theta + mg\sin\theta$. R_{wheel} is the radius of the vehicle wheels and m, ρ, C_d, A_d, g, C_r, and θ are the vehicle mass, the air density, the drag coefficient, the vehicle frontal area, the gravity constant, the rolling resistance coefficient, and the road gradient, respectively. All these parameters are modelled with the data obtained from Autonomie, a software for simulating the performance of different types of vehicles, designed by Argonne National Laboratory [28, 30–32]. The values of the parameters in (8) are all listed in Table 1. Also, in order to express the vehicle acceleration $v'(k)$, (9) and (10) are applied

$$T_{\text{demand}}(k) = \frac{mv'(k) + C_2 v(k)^2 + C_3 + F_{\text{brake}}(k)}{C_1} \tag{8}$$

$$v(k+1) = v(k) + v'(k)\Delta t_k \tag{9}$$

$$v'(k) = \frac{v(k+1) - v(k)}{\Delta t_k} = \frac{v(k+1)^2 - v(k)^2}{2\Delta s} \tag{10}$$

To derive the vehicle motor torque T_{motor}, (11)–(15) are implemented. From Fig. 4, one of the vehicle power flow equations can be expressed by (11), where P_{motor} and P_{gen} represent the motor power and generator power, respectively. Their efficiencies are dependent on the speed and torque values. P_1 denotes the electrical

© The Institution of Engineering and Technology 2018

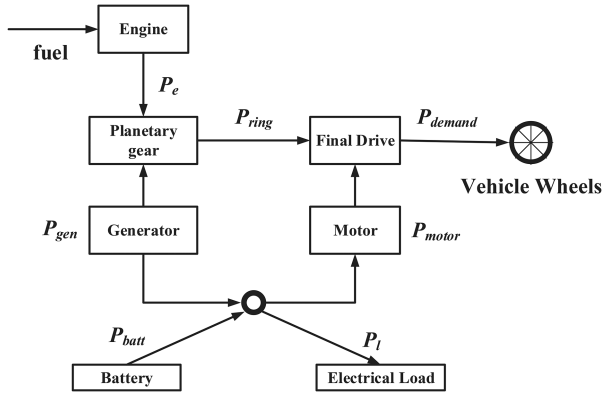

Fig. 4 *Power-split HEV power-flow configuration*

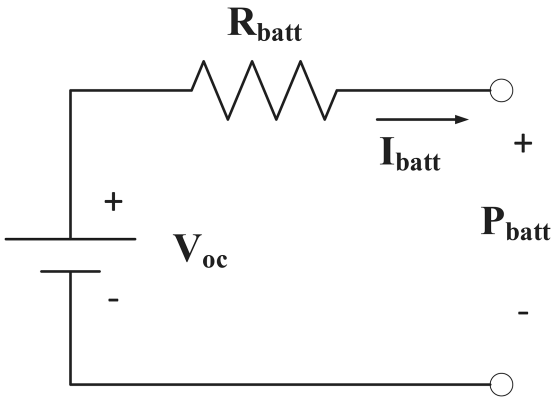

Fig. 5 *HEV battery equivalent circuit*

load which is kept constant. Equation (12) presents the relationship between vehicle motor speed ω_{motor} and ring gear speed ω_{ring}, where γ_{final} represents the final drive ratio and is kept constant. Equation (13) presents the relationship among the generator speed ω_{gen}, the engine speed ω_e, and the motor speed ω_{motor}. Combining (11)–(14), the vehicle motor torque T_{motor} can be derived as in (15)

$$P_{\text{motor}}(k) = P_{\text{batt}}(k) + P_{\text{gen}}(k) - P_{\text{l}} \tag{11}$$

$$\omega_{\text{motor}}(k) = \omega_{\text{ring}}(k) = \frac{v(k)}{R_{\text{wheel}}} \times \gamma_{\text{final}} \tag{12}$$

$$\omega_{\text{gen}}(k) = \left(1 + \frac{1}{\lambda}\right)\omega_e(k) - \frac{1}{\lambda}\omega_{\text{motor}}(k) \tag{13}$$

$$P_{\text{gen}}(k) = T_{\text{gen}}(k)\omega_{\text{gen}}(k) \tag{14}$$

(see (15)) .

Since the expressions for T_{demand} and T_{motor} have both been obtained, the engine torque T_e can be calculated and a detailed expression is presented in the following equation: (see (16)) . Either equality or inequality constraints of each distance step are considered in this paper. For inequality constraints, every control variable (ω_e, P_{batt}, F_{brake} and v) has its own upper and lower bounds, as shown in (17)–(20). In terms of each component in the vehicle powertrain model, both physical and vehicle dynamic constraints are considered. In (12), for example, the rotational speed limits of ω_{motor} which update the limits of $v(k)$, are considered

$$\omega_{e\_\min}(k) \le \omega_e(k) \le \omega_{e\_\max}(k) \tag{17}$$

$$P_{\text{batt\_min}}(k) \le P_{\text{batt}}(k) \le P_{\text{batt\_max}}(k) \tag{18}$$

$$F_{\text{brake\_min}}(k) \le F_{\text{brake}}(k) \le F_{\text{brake\_max}}(k) \tag{19}$$

$$v_{\min}(k) \le v(k) \le v_{\max}(k) \tag{20}$$

Vehicle battery constraints are also taken into consideration. As shown in Fig. 5, an equivalent circuit with an internal resistance R is implemented. V_{oc} stands for the open circuit voltage and I_{batt} represents the battery current. The temperature of the battery is assumed to be constant and the temperature effect is ignored. From the equivalent circuit, (21) can be derived

$$I_{\text{batt}}(k) = \frac{-V_{\text{oc}} + \sqrt{V_{\text{oc}}^2 - 4[P_{\text{batt}}(k)R]}}{2R} \tag{21}$$

$$I_{\text{batt\_min}}(k) \le I_{\text{batt}}(k) \le I_{\text{batt\_max}}(k) \tag{22}$$

In recent years, many papers have been proposed to improve the battery SOC estimation [33–38]. SOC is defined to be the remaining capacity in a battery cell as a percentage of its total capacity [34]. The HEV battery status can be reflected when the vehicle SOC profile is available during the entire trip. Since the battery is an energy storage system with intrinsic chemical properties, it cannot be measured directly [35]. Instead, it can be estimated by the measurement of other variables such as battery voltage and current [37]. It is worth noting that the detailed description of SOC estimation is beyond the scope of this paper. Thus, in (22), the battery current is limited and the initial SOC is pre-set by the author. The SOC expression for the following distance step is presented in (23), where $Q_{\max}$ represents the maximum battery capacity which is kept constant at 4.7 Ah during the whole optimisation.

As in (24), the battery SOC should satisfy the boundary limits in every distance step. In terms of the SOC boundaries, the battery state-of-health (SOH) is taken into consideration. A 100% SOH means it is a fresh battery. The SOH measurement can be derived through other parameters such as battery capacity and internal resistance [35]. Generally, the user needs to change the battery when its capacity is <80% of the rated value. Besides, both excessive charge and discharge should be avoided such that a longer battery life can be obtained. A deep battery depletion could result in less durability and potential degradation [36]. In this paper, therefore, the SOC boundaries are set to be 0.2 and 0.8

$$\text{SOC}(k+1) = \text{SOC}(k) + \frac{I_{\text{batt}}(k)\Delta t_k}{Q_{\max}} \tag{23}$$

$$\text{SOC}_{\min}(k) \le \text{SOC}(k) \le \text{SOC}_{\max}(k) \tag{24}$$

In terms of equality constraints, as shown in Fig. 4, the power-split HEV power flow equations, such as (11), should be satisfied during the entire trip.

$$T_{\text{motor}}(k) = \frac{\{P_{\text{batt}}(k) + [T_e(k)\omega_e(k) + ((T_e(k)\gamma_{\text{final}})/((1+\lambda)R_{\text{wheel}}))v(k)] - P_{\text{l}}\}R_{\text{wheel}}}{v(k)\gamma_{\text{final}}} \tag{15}$$

$$T_e(k) = \frac{\dfrac{1+\lambda}{C_1}\left[m\dfrac{v(k+1)^2 - v(k)^2}{2\Delta s} + C_2 v(k)^2 + C_3 + F_{\text{brake}}(k)\right] - \dfrac{(1+\lambda)R_{\text{wheel}}}{v(k)}(P_{\text{batt}}(k) - P_{\text{l}})}{2\gamma_{\text{final}} - \dfrac{(1+\lambda)R_{\text{wheel}}\omega_e(k)}{v(k)}} \tag{16}$$

© The Institution of Engineering and Technology 2018

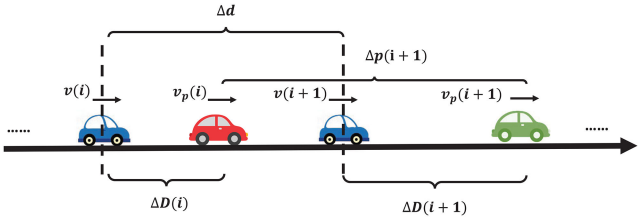

Fig. 6 *Spacing example in the second stage*

2.3 Second stage: speed adaption considering safety spacing

While the vehicle speed is optimised to follow the desired target speed profile, the actual traffic conditions, which may change frequently during the entire long trip, are hardly reflected in the long-term stage. Thus, the distance between the host vehicle and the preceding vehicle of each small segment is considered as a reflection of real traffic conditions in the second stage. No matter whether under heavy or light traffic, this distance should be maintained based on a minimum value, which is named as safety spacing, so that driving safety can be secured. Besides, the distance step in the first stage, Δs, is too wide to be implemented in real time, and the speed variation within the step cannot be detected. Therefore, in the second stage, the distance for each step is divided into smaller segments. For any location n, the number of smaller segments for each Δs is n_s, and the distance value for every small segment Δd is equal to $\Delta s/n_s$.

Let the host vehicle speed at current small segment i be $v_s(n, i)$ and the speed of the preceding vehicle be $v_p(n, i)$, so that the driving distance of the preceding vehicle for the next segment is estimated by

$$\Delta p(n, i+1) \simeq \frac{v_p(n, i) + v_p(n, i+1)}{2} \times \frac{\Delta d}{v_s(n, i)} \tag{25}$$

The distance to the preceding vehicle for the next small segment, $\Delta D(n, i+1)$, is estimated by the current spacing, $\Delta D(n, i)$, and the driving distance of both vehicles (Δp and Δd, respectively), as in (26). In Fig. 6, the blue car represents the host, while the red one or the green one represents the preceding vehicle

$$\Delta D(n, i+1) \simeq \Delta D(n, i) + \Delta p(n, i+1) - \Delta d \tag{26}$$

The safety distance should take several elements into account, including the preceding vehicle's performance, road conditions, braking capabilities, and so on. It is worth noting that the host vehicle does not have to follow the same vehicle at all locations. No matter what type of the preceding vehicle is, for each fine segment, the safety distance to the preceding vehicle is updated. In this paper, a safety distance policy [39] is adopted for modelling the safety spacing. As in the following equation, the safety distance ΔD_{ss} for the next small segment is

$$\Delta D_{\text{ss}}(n, i+1) \simeq h_1[v_s(n, i)^2 - v_p(n, i)^2] + h_2 v_p(n, i) + h_3 \tag{27}$$

where h_1, h_2, h_3 are positive constants determined by the specified values of human reaction time, and the vehicle's full acceleration and braking capabilities [40].

Equation (28) maintains this safety spacing for the next small segment. The value of $\Delta D(n, i+1)$ should be wider than or at least equal to the desired safety distance

$$\Delta D(n, i+1) \geq \Delta D_{\text{ss}}(n, i+1) \tag{28}$$

Besides, the vehicle speed should not exceed the given speed limits at any fine location. Therefore, the desired host vehicle safety speed v_{ss} for the next small segment can be calculated. In (29), the optimal speed generated from the first stage $v_{\text{first}}(n, i+1)$ at the next fine location and the calculated safety speed value are all considered.

Thus, the optimal speed generated in the first stage and the safety speed derived in the second stage are compared, then the new target speed for the host vehicle in the next short segment, $v'_{\text{target}}(n, i+1)$, can be determined. If the optimal speed profile generated in the first stage is lower than the safety speed, the target speed is maintained and the host vehicle follows it. However, if the optimal speed is higher than the safety speed, the target speed is regulated without exceeding the safety speed.

The cost function of the speed adaption considering safety spacing is described by (30). ω_3 and ω_4 are weighting terms, and both vehicle consumption cost and speed deviation are under a smaller scale. Moreover, since the second stage is an en-route adaption, it is assumed that the driver is concerned about the driving strategy for only the next short horizon, meaning J_{local} is minimised only for the next small distance step.

3 EDA application

In this paper, the final objective functions of both stages are non-linear and complicated with different control inputs. An EDA is utilised for solving these optimisation problems. In order to compare the simulation results and demonstrate the feasibility, robustness, and effectiveness of the proposed HEV model, a GA is also implemented and its results are set to be the benchmark. Either of the EDA or GA can optimise this problem while considering constraints from various perspectives. However, the computational cost by GA is much greater than that of the same objective function reached by using an EDA.

EDAs are evolutionary algorithms on the basis of global statistical information extracted from promising solutions. It is a stochastic optimisation method that builds a probability distribution from promising populations by applying a probability distribution model. The probability-based generation of samples in an EDA can accelerate optimisation and present an explicit structure to the problem.

For this hierarchical optimisation problem, some details are shown in Fig. 7. Despite pre-trip optimisation being performed before the HEV's departure, the computational cost should not be too large. The following approaches are implemented for shortening the computing time. First, the initial populations are generated by the estimated feasible solution area instead of random generation. Considering the physical limits and general information from the HEV drivetrain, the feasible solution can be estimated. For example, in the initial generation, the mean values of control inputs can be simply assumed by the linear vehicle acceleration and deceleration in speed transition regions. Second, a large number of population is preferred such that the promising populations are selected at early iterations. Meanwhile, a smaller truncation ratio could lead to more population replacement such that the objective function value tends to decrease and converge efficiently [41]. Some EDA parameter settings are presented in [42]. In this pre-trip optimisation problem, t_r is set to be 0.3 while n_{pop} is 400. In this case, the truncation ratio is relatively small and the population size is adequate

$$v'_{\text{target}}(n, i+1) \leq \min\left\{v_{\text{first}}(n, i+1), \sqrt{\frac{h_1 v_p^2(n, i) - h_2 v_p(n, i) - h_3 + \Delta D(n, i+1)}{h_1}}\right\} \tag{29}$$

$$\min J_{\text{local}}(n, i) = \omega_3 m_f(n, i)\Delta t(n, i) + \omega_4[v_s(n, i) - v'_{\text{target}}(n, i+1)]^2 \tag{30}$$

$$\Delta t(n, i) = t(n, i+1) - t(n, i) = \frac{2\Delta d}{v_s(n, i) + v_s(n, i+1)} \tag{31}$$

The author selects an EDA for solving this problem due to its robustness for non-linear and complex optimisation problems with few parameters to control. Moreover, the performance of an EDA is not largely affected by the size of the problem, nor the limits of computer memory. Compared with other approaches, an EDA is

© The Institution of Engineering and Technology 2018

able to maintain a lower computational cost without adjusting too many system parameters [43].

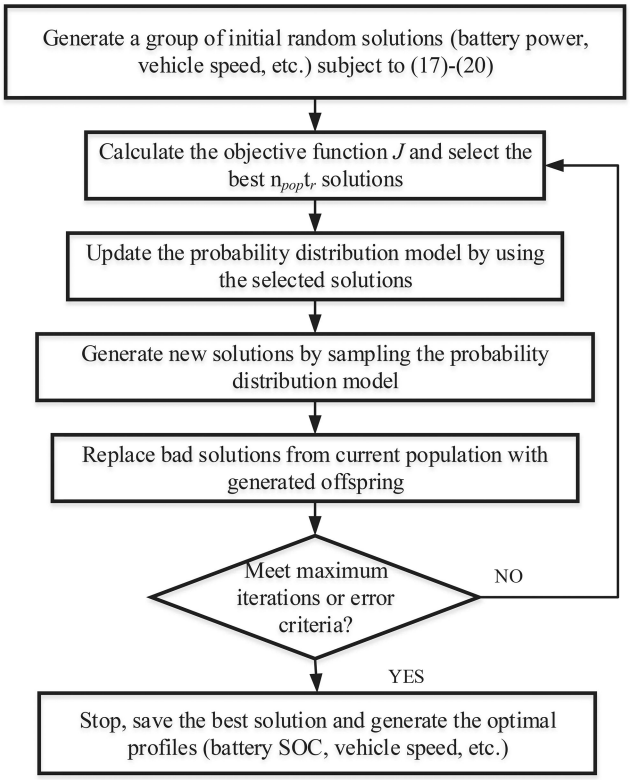

Fig. 7 *Flowchart of EDA*

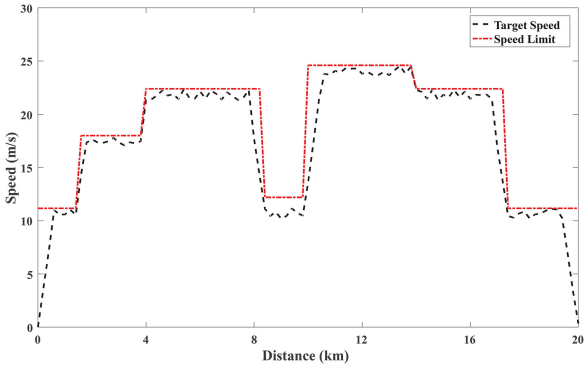

Fig. 8 *Target speed profile in pre-trip optimisation*

Table 2 Diverse values of ω_1

ω_1	ω_2	Fuel consumption, g	Final SOC
10^5	2	366	0.243
3×10^5	2	352	0.224
5×10^5	2	342	0.219
7×10^5	2	337	0.204
8×10^5	2	332	0.200

Table 3 Diverse values of ω_2

ω_1	ω_2	Fuel consumption, g	Speed deviation, %
8×10^5	0.1	304	1.74
8×10^5	0.5	317	1.32
8×10^5	1	321	1.27
8×10^5	2	332	1.12
8×10^5	4	341	0.95

4 Result analysis

All proposed simulations are run on an Intel(R) Core(TM) i7-4712HQ CPU @ 2.30 GHz, 16.0 GB, Windows 8.1, and solved by Matlab 2017b. As presented in the previous section, the authors use an EDA to perform the hierarchical simulation.

4.1 Generations of long-term optimisation before departure

To generate a reasonable target speed profile and determine the values of weighting factors, several trials are performed. The driving route under the test is 20 km long and the identical distance step Δs is 200 m. Consequently, the number of distance steps is 101. The initial SOC is set as 0.6 and the boundaries are set as 0.2–0.8. It is assumed that no charging station is available during the entire trip.

Based on the speed limits and historic average speed of every distance step under smooth traffic condition, the initial target speed is given in Fig. 8 and it is only used as a reference file for this optimisation. This target speed profile is not optimised through the cost function but it is sufficient and appropriate enough to make comparisons and demonstrate the advantage of the optimised speed profile.

In the pre-trip optimisation, the first term mainly controls the fuel consumption while the second term regulates the speed deviation. The unit and magnitude for each term is different. Therefore, two weighting factors ω_1 and ω_2 are used for normalisation. In this study, the environmental effect is considered. The electric power stored in the battery has priority over exhaust gas. If the required energy for the entire trip can be convered by the current battery power, then a vehicle is able to finish the trip without consuming any fuel. Otherwise, the electric power of the battery should be used till the SOC reaches allowable lower limit. To reach this energy priority, simulations for diverse ω_1 were conducted with a fixed value of $\omega_2 = 2$. As shown in Table 2, when ω_1 increases, the total fuel consumption is decreased. However, when ω_1 is smaller than 8×10^5, the final value of SOC does not reach its minimum, which means there is still electric energy in the battery available for use. Thus, the value of weighting factor ω_1 is set to be 8×10^5.

In order to determine the appropriate value of ω_2, the trials of ω_2 values are carried out while ω_1 remains the same. ω_2 reflects how the target speed is followed at every location and, as a result, the balance between total fuel consumption and vehicle speed deviation. As shown in Table 3, despite the starting acceleration and ending deceleration segments, when the second weighing term ω_2 is <2, the average speed deviation to the target speed is more than 1%. As ω_2 increases, the optimised speed profile is closer to the target speed profile and results in higher fuel consumption. Since the traffic is assumed to be light in the pre-trip stage, it is not suitable if the speed deviation is large, namely, a vehicle is driven at a relatively low speed. Thus, situations in which only ω_2 is equal to or larger than 2 are considered. In this first stage simulation, ω_2 is set to be 4 in order to reach a balanced driving condition. The final speed of the entire driving cycle should be zero. This is implemented by adding another term $\omega_3(v(N+1)-0)$ into the function and setting ω_3 to be 10^8, which is large enough to act as a penalty.

For the pre-trip optimisation, the maximum iteration n_{iter} is set to be 300. The population size is set as 400. Instead of random selections, our initial populations are generated based on the vehicle drivetrain model and a regulated speed profile where the vehicle accelerates linearly at the beginning, maintains at speed limits during the trip, and finally stops with linear deceleration. As a comparison, the input boundary values are also performed as the other initial condition. As in Fig. 9, the blue and green dotted lines illustrate the convergence under both initial conditions. Typical final fitness values and corresponding iteration numbers are also marked. After the 1st iteration, a lower objective value is obtained when the promising populations are used and the final value converges around 200th iterations. When starting with boundary values, the final fitness value is also reached around 223rd

© The Institution of Engineering and Technology 2018

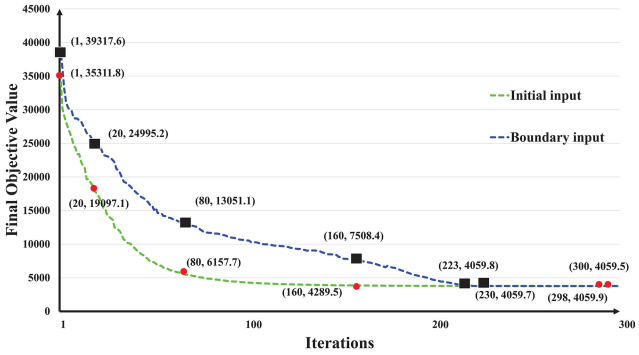

Fig. 9 *Convergence tendency of the EDA method*

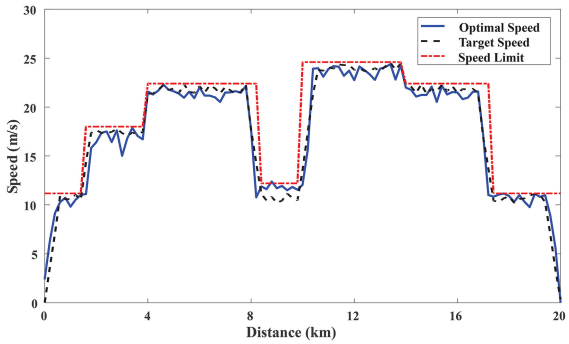

Fig. 10 *Optimal speed profile in the first stage optimisation*

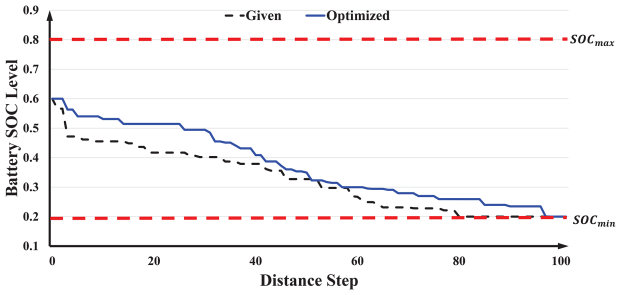

Fig. 11 *Vehicle SOC profile in the first stage optimisation*

Table 4 Comparison of simulation results

	Fuel consumption, g	Driving time, s	Maximum speed deviation, %
EDA	341	1391	4.2
target profile	363	1373	/

iterations. However, the starting value is higher, and the convergence rate is relatively lower. This result shows a promising solution is able to speed up the optimisation process and the proposed first stage optimisation has the capability of obtaining solutions with good qualities and convergence rate with stable characteristics.

Fig. 10 shows the optimal speed profiles generated for the test route in the first stage. The solid blue line represents the speeds optimised by the EDA. The dotted red and black lines represent the speed limits, and the target speeds, respectively. In general, the overall optimised speeds follow the target speed pattern, and never exceed the speed limits during the entire trip.

Fig. 11 presents the vehicle SOC levels for the entire route. In every distance step, the value is maintained within the boundaries (0.2–0.8) and both SOC curves drop down to the minimum value in the end. In the target profile, the SOC level reaches the allowable minimum around 80th step and there is still about 4 km away from the destination. However, when the EDA optimisation is applied, the SOC level maintains above the minimum until the arrival, such that the battery energy is reasonably consumed during the trip.

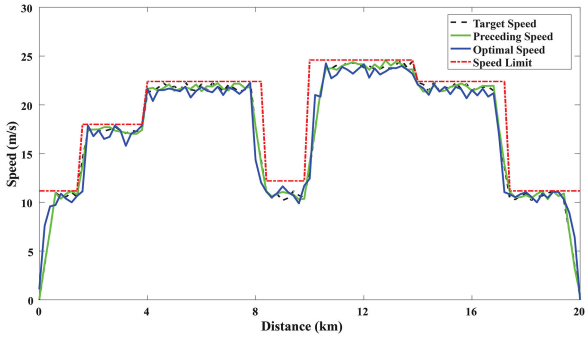

Fig. 12 *Preceding and host vehicle speed profiles under smooth traffic*

Table 4 lists the typical driving results in the long-term optimisation. By using the EDA, the average estimated fuel consumption is 341 g, the average total driving time is 1391 s, while these values are 363 g, 1373 s by using the reference profile, respectively. The fuel consumption is reduced by 6.1% in EDA while the average total driving times are almost identical in the range with no more than a 2% difference. The maximum speed deviation is <5%, which indicates the optimised speed follows the target speed adequately.

4.2 Speed adaption considering changes in traffic conditions

The previous stage optimisation is performed before departure and traffic condition is assumed to be light. In the second stage, considering the real changes in traffic condition, speed adaption is conducted for each short horizon. The number of smaller segments n_s for each Δs is set to be 5. As a consequence, the distance value for every small segment Δd is 40 m in the second stage simulation. Similar to the first stage analysis, the values of weighting terms ω_3 and ω_4 are set to 10^7 and 5, respectively. However, both the optimal speed generated from the first stage and the calculated safety speed are compared to determine the target speed in the second stage. In order to adapt the host vehicle based on the pre-trip optimisation results, it is assumed that the preceding vehicle and the host vehicle are the same type of power-split HEV so that the constraints caused by the drivetrain characteristics are still valid, and both vehicles go through the same driving cycle.

The speed profile of the preceding vehicle is assumed to be measured. Fig. 12 illustrates the preceding vehicle speed, the adapted host vehicle speed determined by the EDA under smooth traffic condition. In this case, most target speed does not need to be regulated since the host vehicle can follow the preceding vehicle under a near-steady state. The velocity difference between two vehicles is <5% so that the spacing between the two vehicles can be maintained. The optimised fuel consumption of the host vehicle is 345 g and total driving time is 1375 s.

The actual spacing to the preceding vehicle is calculated in the second stage. The initial distance between the two vehicles is set to be 8 m. The final spacing is set to be 0 m because the same driving route is applied to both vehicles. This value does not indicate a collision, but implies they have the same destination. Fig. 13 presents the actual spacing during the entire driving cycle. The results indicate that the spacing to the preceding vehicle is always guaranteed.

Fig. 14 demonstrates the driving results under heavy traffic condition. The preceding vehicle is slowed down around 5–7 and 14–16 km, which indicates the traffic is congested. The target speed is correspondingly adapted around these areas. The fuel consumption is 365 g and the total driving time increases to 1520 s. In the time domain, the target speed profiles after the congested area need to be calculated again. In this scenario, two congested areas lead to at least two recalculations. However, in the distance domain, except the adapted area, the remaining target speed profile is slightly affected and remains valid compared with the optimal speed results from first stage. This demonstrates the advantage of using the distance domain.

Under heavy traffic, the safety spacing becomes larger. However, the actual distance to the preceding vehicle is not

© The Institution of Engineering and Technology 2018

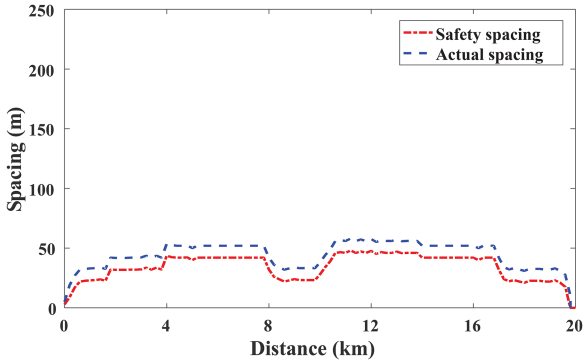

Fig. 13 *Actual spacing to the preceding vehicle under smooth traffic*

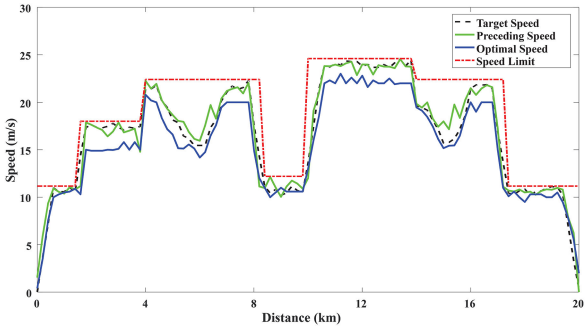

Fig. 14 *Preceding and host vehicle speed profiles under heavy traffic*

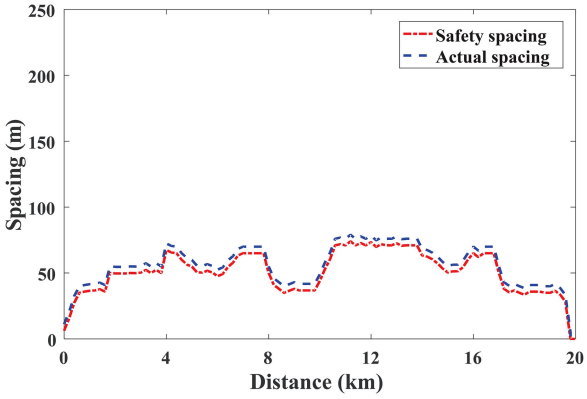

Fig. 15 *Actual spacing to the preceding vehicle under heavy traffic*

necessary to be very large. Fig. 15 implies that the difference between safety and actual spacing still guarantees the driving safety during the whole trip.

5 Conclusion

In this paper, the authors investigate a distance-based hierarchical control and ecological driving strategy for a power-split HEV by implementing an EDA. A vehicle powertrain model is mathematically constructed. The first stage aims to optimise the vehicle fuel cost and the speed deviation, which is constrained by the vehicle powertrain limits, road conditions, and speed limits. In the second stage, an en-route speed adaption is performed. The distance to the preceding vehicle for each short horizon is considered to be an indicator of real traffic conditions. For both stages, an EDA is utilised and a GA is set to be the benchmark. The simulation results of both stages demonstrate the feasibility, robustness, and effectiveness of the proposed power-split HEV model.

The computational cost either for pre-trip optimisation or the en-route speed adaption can be improved or tailored to realise real-time implementation. Emergence conditions such as sudden acceleration or deceleration to avoid accidents can be considered. To evaluate the proposed method in a more realistic environment, a hardware in the loop (HIL) testing platform can be considered in the future. In the HIL, components of the HEV system model can be substituted by real system components. Besides, such HIL testing platform will allow developers to validate new hardware and software HEV solutions in a more integrated environment. The optimal mechanism for dividing the distance segment for reaching more accurate results while maintaining the computational cost, an enhanced selection of the initial feasible solution under the distance domain will be further investigated in the future.

6 Acknowledgment

This work was in part supported by the U.S. Department of Energy Graduate Automotive Technology Education under grant DE-EE0005565 and the Basic Science Research Program through the National Research Foundation of Korea (NRF-2016R1D1A1B03935190). The authors thank the anonymous reviewers for their valuable comments and suggestions to improve the quality of this paper.

7 References

[1] Murphey, Y.L., Park, J., Chen, Z., *et al.*: 'Intelligent hybrid vehicle power control – Part I: machine learning of optimal vehicle power', *IEEE Trans. Veh. Technol.*, 2012, **61**, (8), pp. 3519–3530

[2] Malikopoulos, A.A.: 'Supervisory power management control algorithms for hybrid electric vehicles: a survey', *IEEE Trans. Intell. Transp. Syst.*, 2014, **15**, (5), pp. 1869–1885

[3] Denis, N., Dubois, M.R., Trovão, J.P.F., *et al.*: 'Power split strategy optimization of a plug-in parallel hybrid electric vehicle', *IEEE Trans. Veh. Technol.*, 2018, **67**, (1), pp. 315–326

[4] Ramadan, H.S., Becherif, M., Claude, F.: 'Energy management improvement of hybrid electric vehicles via combined GPS/rule-based methodology', *IEEE Trans. Autom. Sci. Eng.*, 2017, **14**, (2), pp. 586–597

[5] Li, Y., Chen, B.: 'Development of integrated rule-based control and equivalent consumption minimization strategy for HEV energy management'. 2016 12th IEEE/ASME Int. Conf. Mechatronic and Embedded Systems and Applications (MESA), Auckland, New Zealand, August 2016, pp. 1–6

[6] Li, S.G., Sharkh, S.M., Walsh, F.C., *et al.*: 'Energy and battery management of a plug-in series hybrid electric vehicle using fuzzy logic', *IEEE Trans. Veh. Technol.*, 2011, **60**, (8), pp. 3571–3585

[7] Padmarajan, B.V., McGordon, A., Jennings, P.A.: 'Blended rule-based energy management for PHEV: system structure and strategy', *IEEE Trans. Veh. Technol.*, 2016, **65**, (10), pp. 8757–8762

[8] Hui, X., Ding, Y.: 'The study of plug-In hybrid electric vehicle power management strategy simulation'. IEEE 2008 Vehicle Power and Propulsion Conf.. VPPC'08, Harbin, China, 2008, pp. 1–3

[9] Prokhorov, D.V.: 'Toyota Prius HEV neurocontrol and diagnostics', *Neural Netw.*, 2008, **21**, (2–3), pp. 458–465

[10] Jiang, Q., Ossart, F., Marchand, C.: 'Comparative study of real-time HEV energy management strategies', *IEEE Trans. Veh. Technol.*, 2017, **66**, (12), pp. 10875–10888

[11] Rezaei, A., Burl, J.B., Zhou, B.: 'Estimation of the ECMS equivalent factor bounds for hybrid electric vehicles', *IEEE Trans. Control Syst. Technol.*, 2017, **26**, pp. 2198–2205

[12] Sun, C., Sun, F., He, H.: 'Investigating adaptive-ECMS with velocity forecast ability for hybrid electric vehicles', *Appl. Energy*, 2017, **185**, pp. 1644–1653

[13] Zhao, D., Stobart, R., Dong, G., *et al.*: 'Real-time energy management for diesel heavy duty hybrid electric vehicles', *IEEE Trans. Control Syst. Technol.*, 2015, **23**, (3), pp. 829–841

[14] Guo, L., Gao, B., Gao, Y., *et al.*: 'Optimal energy management for HEVs in Eco-driving applications using bi-level MPC', *IEEE Trans. Intell. Transp. Syst.*, 2017, **18**, (8), pp. 2153–2162

[15] Zhang, J., Shen, T.: 'Real-time fuel economy optimization with nonlinear MPC for PHEVs', *IEEE Trans. Control. Syst. Technol.*, 2016, **24**, (6), pp. 2167–2175

[16] Liu, B., Li, L., Wang, X., *et al.*: 'Hybrid electric vehicle downshifting strategy based on stochastic dynamic programming during regenerative braking process', *IEEE Trans. Veh. Technol.*, 2018, **67**, pp. 4716–4727

[17] Xu, F., Jing, Y., Jiao, X.: 'A modified energy management strategy based on SDP policy iteration for commuter hybrid electric vehicles'. 2016 35th Chinese Control Conf. (CCC), Chengdu, China, July 2016, pp. 2537–2541

[18] Zhang, C., Vahid, A.: 'Real-time optimal control of plug-in hybrid vehicles with trip preview'. American Control Conf. (ACC), Baltimore, MD, USA, June 2010, pp. 6917–6922

[19] Zhao, J., Wang, J.: 'Integrated model predictive control of hybrid electric vehicles coupled with after treatment systems', *IEEE Trans. Veh. Technol.*, 2016, **65**, (3), pp. 1199–1211

[20] Sun, C., Moura, S.J., Hu, X., *et al.*: 'Dynamic traffic feedback data enabled energy management in plug-in hybrid electric vehicles', *IEEE Trans. Control Syst. Technol.*, 2015, **23**, (3), pp. 1075–1086

[21] Enang, W., Bannister, C.: 'Modelling and control of hybrid electric vehicles (a comprehensive review)', *Renew. Sust. Energy Rev.*, 2017, **74**, pp. 1210–1239

[22] HomChaudhuri, B., Lin, R., Pisu, P.: 'Hierarchical control strategies for energy management of connected hybrid electric vehicles in urban roads', *Transp. Res. C, Emerg. Technol.*, 2016, **62**, pp. 70–86

© The Institution of Engineering and Technology 2018

[23] Huang, M.: 'Optimal multilevel hierarchical control strategy for parallel hybrid electric vehicle'. IEEE Vehicle Power and Propulsion Conf., 2006. VPPC'06, Windsor, UK, September 2006, pp. 1–4
[24] Wang, X., Li, L., Yang, C.: 'Hierarchical control of dry clutch for engine-start process in a parallel hybrid electric vehicle', *IEEE Trans. Transp. Electrification*, 2016, **2**, (2), pp. 231–243
[25] Mensing, F., Bideaux, E., Trigui, R., *et al.*: 'Trajectory optimization for eco-driving taking into account traffic constraints', *Transp. Res. D, Transp. Environ.*, 2013, **18**, pp. 55–61
[26] Cheng, Q., Nouveliere, L., Orfila, O.: 'A new eco-driving assistance system for a light vehicle: energy management and speed optimization'. 2013 IEEE Intelligent Vehicles Symp. (IV), Gold Coast, Australia, June 2013, pp. 1434–1439
[27] Malikopoulos, A.A.: 'A multiobjective optimization framework for online stochastic optimal control in hybrid electric vehicles', *IEEE Trans. Control Syst. Technol.*, 2016, **24**, (2), pp. 440–450
[28] Montazeri-Gh, M., Mahmoodi-k, M.: 'Development a new power management strategy for power split hybrid electric vehicles', *Transp. Res. D, Transp. Environ.*, 2015, **37**, pp. 79–96
[29] Duoba, M., Lohse-Busch, H., Carlson, R., *et al.*: 'Analysis of power-split HEV control strategies using data from several vehicles' (No. 2007-01-0291). SAE Technical Paper, 2007
[30] Argonne National Laboratory, AUTONOMIE, Available at http://www.autonomie.net
[31] Kim, N., Rousseau, A., Rask, E.: 'Autonomie model validation with test data for 2010 Toyota Prius'. in Proc. SAE, Detroit, MI, USA, 2012, pp. 1–14
[32] Kim, N., Duoba, M., Kim, N., *et al.*: 'Validating Volt PHEV model with dynamometer test data using autonomie', *SAE Int. J. Passenger Cars-Mech. Syst.*, 2013, **6**, (2013-01-1458), pp. 985–992
[33] Yanli, L., Dai Sheng, C.Z.: 'Estimation of state of charge of lithium-ion battery based on finite difference extended Kalman filter', *Trans. China Electrotech. Soc.*, 2014, **29**, (1), pp. 221–228
[34] Sepasi, S., Ghorbani, R., Liaw, B.Y.: 'SOC estimation for aged lithium-ion batteries using model adaptive extended Kalman filter'. 2013 IEEE Transportation Electrification Conf. Expo (ITEC), Detroit, MI, USA, June 2013, pp. 1–6
[35] Cuma, M.U., Koroglu, T.: 'A comprehensive review on estimation strategies used in hybrid and battery electric vehicles', *Renew. Sust. Energy Rev.*, 2015, **42**, pp. 517–531
[36] Sun, Y., Ma, Z., Tang, G., *et al.*: 'Estimation method of state-of-charge for lithium-ion battery used in hybrid electric vehicles based on variable structure extended kalman filter', *Chin. J. Mech. Eng.*, 2016, **29**, (4), pp. 717–726
[37] Chun, C.Y., Seo, G.S., Cho, B.H., *et al.*: 'A fast state-of-charge estimation algorithm for LiFePO 4 batteries utilizing extended Kalman filter'. 2013 IEEE ECCE Asia Downunder (ECCE Asia), Melbourne, VIC, Australia, June 2013, pp. 912–916
[38] Baba, A., Adachi, S.: 'SOC estimation of HEV/EV battery using series Kalman filter', *Electr. Eng. Jpn.*, 2014, **187**, (2), pp. 53–62
[39] Chien, C., Lai, M., Mayr, R.: 'Vehicle following controller design for autonomous intelligent vehicles'. In Conf. Intelligent Robots in Factory, Field, Space, and Service, Houston, TX, USA, March 1994, p. 1203
[40] Chien, C.C., Zhang, Y., Cheng, C.Y.: 'Autonomous intelligent cruise control using both front and back information for tight vehicle following maneuvers'. Proc. 1995 American Control Conf., Seattle, WA, USA, 1995, vol. 5, pp. 3091–3095
[41] Yang, P., Tang, K., Lu, X.: 'Improving estimation of distribution algorithm on multimodal problems by detecting promising areas', *IEEE Trans. Cybernetics*, 2015, **45**, (8), pp. 1438–1449
[42] Qi, X., Wu, G., Boriboonsomsin, K., *et al.*: 'Development and evaluation of an evolutionary algorithm-based online energy management system for plug-in hybrid electric vehicles', *IEEE Trans. Intell. Transp. Syst.*, 2017, **18**, (8), pp. 2181–2191
[43] Su, W., Chow, M.Y.: 'Performance evaluation of an EDA-based large-scale plug-in hybrid electric vehicle charging algorithm', *IEEE Trans. Smart Grid*, 2012, **3**, (1), pp. 308–315

© The Institution of Engineering and Technology 2018